Supporting Information

Pongprayoon et al. 10.1073/pnas.0907315106

SI Methods

To compute the standard free energy of binding ΔG^0 or equivalently, the dissociation constant K_d, we follow a recently developed method by Henchman and coworkers (1). The two quantities of interest are related by $K_d = V^0 \exp(-\Delta G^o/RT)$ where $V^0 = 1.661$ nm^3 is the standard volume corresponding to a standard concentration of 1 M. The original derivation assumes that a potential of mean force (PMF) is sampled along a 1D reaction coordinate such as the channel axis along z, whereas at the same time orthogonal movement is restricted by a harmonic confinement potential. Here, we do not employ such a potential but use the fact that simulations with periodic boundary conditions also provide the confinement necessary to formally evaluate the statistical mechanical integrals. In this case, ΔG^0 can be computed as the sum

$$\Delta G^0 = \Delta G_{\mathrm{PMF}} + \Delta G_{\mathrm{V}}$$

of the free energy change of binding between the ligand-bound and unbound state based on the PMF and the free energy change from unbound volume to standard-state volume; the term ΔG_{R} in the original equation 6 in ref. 1 vanishes because there is no change in free energy associated with the introduction of confinement restraints. The final standard binding free energy is then

$$\Delta G^0 = \Delta W - RT \ln \frac{l_b A_u}{\nu V^0}$$

where all terms are computed as in the original formulation except for A_u, which has the value of the average cross sectional area of the simulation box perpendicular to the membrane normal, and the number of particles ν that were sampled in the same umbrella simulations ($\nu = 3$, in the present case). The depth of the binding site, ΔW, is calculated as an exponential average over the unbound region of the PMF $W(z)$,

$$\Delta W = \ln\langle \exp(-[W(z) - \min_z W(z)]/RT \rangle_{\mathrm{unbound}}.$$

We defined the bound state by inspecting the PMF to be the region -3.4 Å $\leq z \leq 3.4$ Å (and hence, the unbound region contains all data points with $z < -3.4$ Å and $z > 3.4$ Å), but the value of the binding free energy is generally insensitive to the exact boundaries due to the exponential average. For consistency and to reflect the geometry of the OrpP pore, we used the same definition of the binding site for both chloride and phosphate; choosing a chloride site between -1 and 3.4 nm gives virtually the same values. The bound length l_b is a configurational integral of the PMF over the bound state and computed as

$$l_b = \int_{\mathrm{bound}} \exp(-[W(z) - \min_z W(z)]/RT) dz.$$

The error on the observables ΔG^0 and K_d were calculated from the SD of the PMFs (from block averaging over three 200-ps blocks) and the PMFs themselves. With the assumption that the data on each data point of the PMF, $W(z)$, are normally distributed with mean $W(z)$ and width equal to the SD, $N = 10{,}000$ PMFs were randomly sampled. Observables were calculated from these N PMFs as described above. The reported values are the mean and SD of these N samples. The error estimation procedure converged for $N > 1{,}000$ samples.

The error for the selectivity, $K_d(\mathrm{Cl}^-)/K_d(\mathrm{PO_4}^{3-})$, as calculated via error propagation from the errors on the dissociation constants, is 1.2 for a 7.3-fold stronger binding of phosphate over chloride.

1. Doudou S, Burton NA, Henchman RH (2009) Standard free energy of binding from a one-dimensional potential of mean force. *J Chem Theory Comput* 5:909–918.
2. Smart OS, Neduvelil JG, Wang X, Wallace BA, Sansom MSP (1996) HOLE: A program for the analysis of the pore dimensions of ion channel structural models. *J Mol Graphics* 14:354–360.

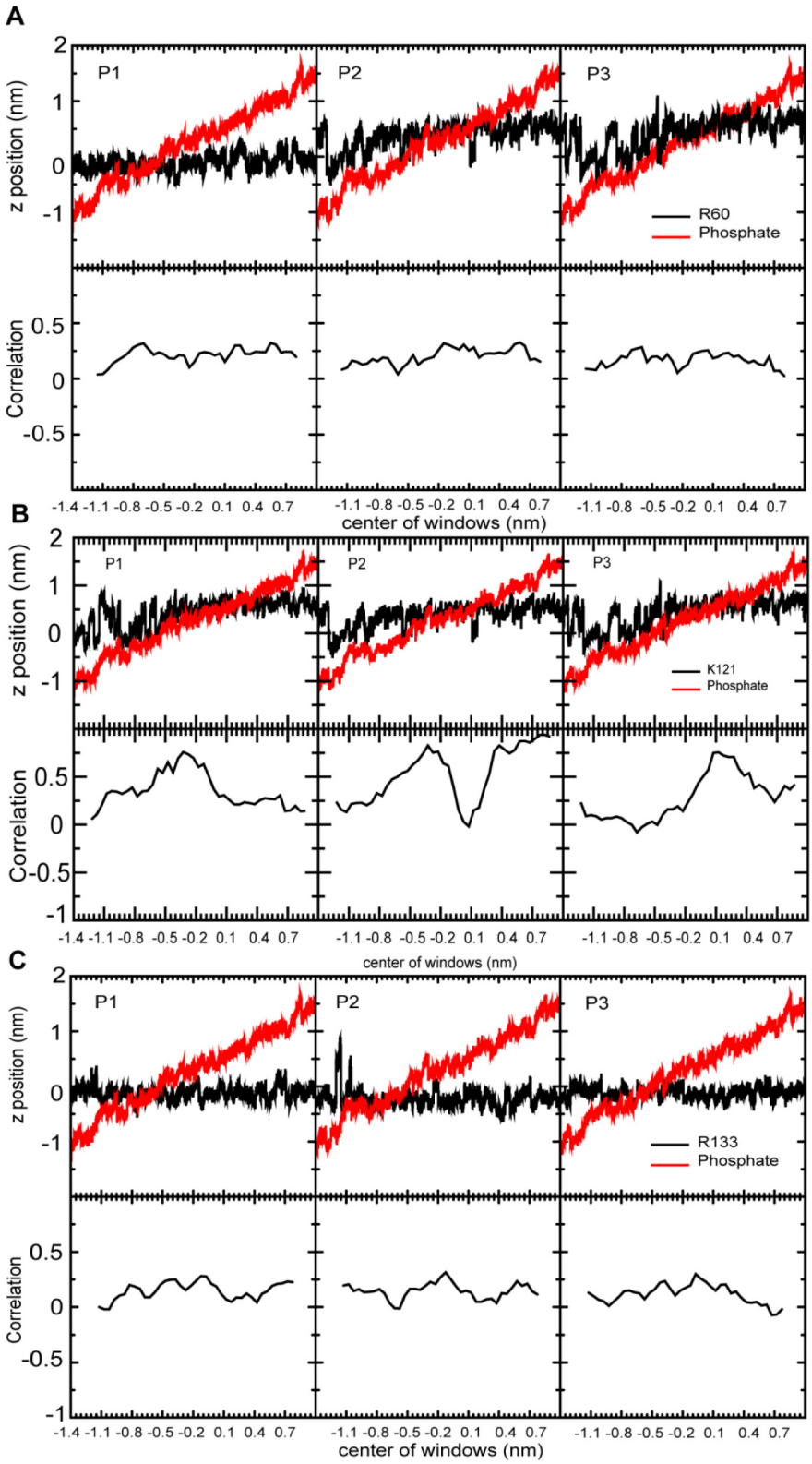

Fig. S1. Correlation between the phosphate ion and pore lining basic side chains. (*A*–*C*) The *z*-position of the ion together with the position of the N_ε of the lysine or the center of mass of the guanidino groups of the arginine residues. Data are shown for each monomer separately (*Upper*). Correlation coefficients between the positions in each umbrella window (*Lower*). Data are smoothed with a running average over six windows. (*A*) R60; (*B*) K121; (*C*) R133.

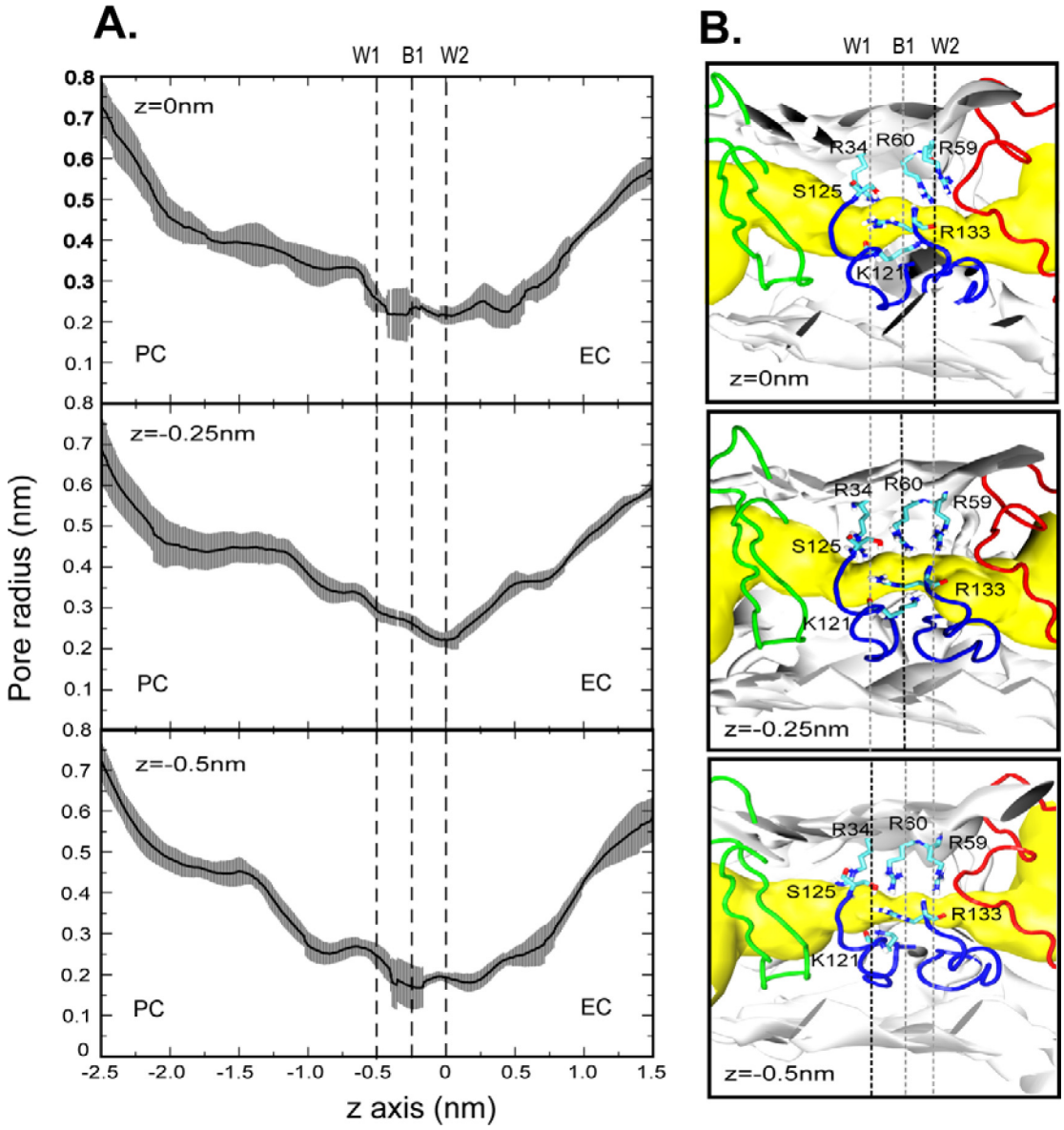

Fig. S2. Flexibility of the OprP pore. (*A*) Average pore profiles of a OprP monomer with phosphate present at $z = 0$ (W2), -0.25 (B1), and -0.5 (W1) nm, created with HOLE (2). (*B*) shows pore-lining surfaces which are scaled and aligned to correspond to the pore profile above with a presence of R34, R59, R60, K121, S125, and R133. The black dash line represents a phosphate position.

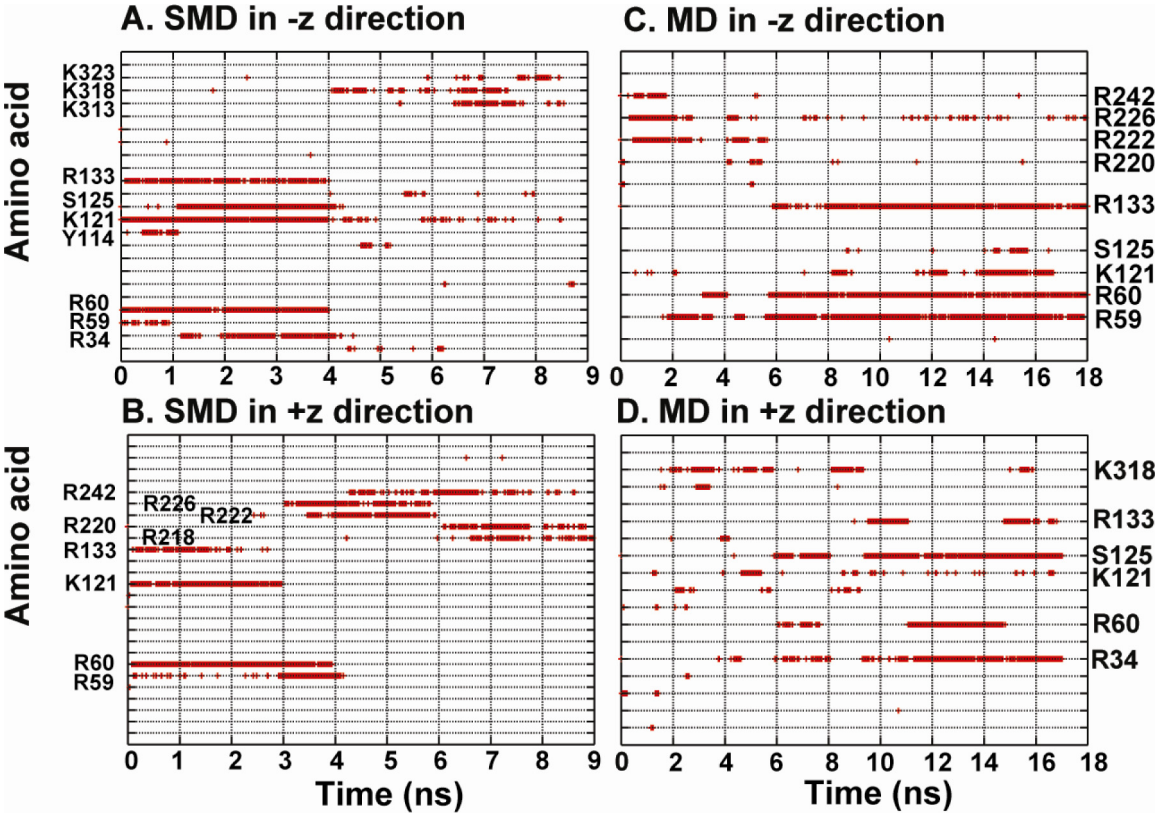

Fig. S3. Time-resolved hydrogen bond existence between the phosphate and the pore-lining amino acids during molecular dynamics (MD). Hydrogen-bonding network resulting from steered (S)MD (*A* and *B*), and from unbiased MD simulations in both $-z$ and $+z$ directions (*C* and *D*).

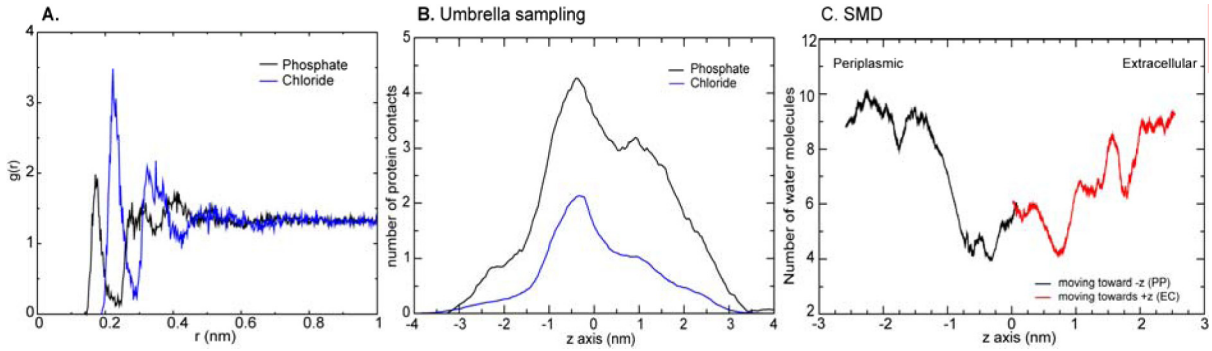

Fig. S4. Analysis of hydration of phosphate and chloride anions reveals differential desolvation in the OprP pore. (*A*) Radial distribution function $g(r)$ of water oxygen around the anion in bulk water. The Pi first hydration shell is characterized by a water oxygen-anion center of mass distance $r < 0.275$ nm, and the one of chloride by $r < 0.3$ nm. (*B*) Average number of contacts (distance, <0.3 nm) between anion and protein from the umbrella sampling simulations. (*C*) Number of water molecules in the first hydration shell of phosphate from the SMD simulations starting at the center. The SMD data agree with the ones derived from umbrella sampling (Fig. 5).